FACTA UNIVERSITATIS
Series: **Automatic Control and Robotics** ONLINE FIRST
https://doi.org/10.22190/FUACR240501001M

Regular Paper

ADAPTATION OF THE FEEDBACK TRANSFER FUNCTION FOR OSICILATION BASED TESTING OF SECOND-ORDER ACTIVE RC FILTERS

UDC ((004.3/.4:0.034.2)+004.78)

Dejan Mirković, Miljana Milić, Milena Stanojlović Mirković

University of Niš, Faculty of Electronic Engineering, Department of Electronics, Republic of Serbia

ORCID iD: Dejan Mirković https://orcid.org/0000-0001-5877-1404
Miljana Milić https://orcid.org/0000-0001-7037-7709
Milena Stanojlović Mirković https://orcid.org/0000-0002-0935-6922

Abstract. *This paper, explores possible solutions for the feedback transfer functions applied in active RC filters for oscillation-based testing (OBT). Three types of filter transfer functions, namely low-pass (LP), high-pass (HP) and band-pass (BP) are examined. Active filters are realized with the realistic operational amplifier model targeting the 180nm CMOS technology. To confirm the theoretical insights, three realizations of LP, HP, BP second-order filterers with proposed feedbacks are designed and simulated. One of the solutions, namely the BP filter, is further examined by inserting defects in the circuit. Based on the time domain simulations, the key parameters are extracted from the oscillating filter's output signal. The fault dictionary has been created and appropriate classification of the defects is performed.*

Key words: *Feedback loop, active RC filters, transfer function, oscillation-based testing, fault dictionary.*

1. INTRODUCTION

High reliability of the contemporary electronic systems is in a high demand. Following the "more than Moor" law, these systems increase in size and complexity [1]. As a result, the testing structures should follow the same trend. However, more complex testing structures introduce additional costs in both time and resources. While the digital circuitry testing techniques are well established [2], testing of the analog circuitry is particularly

Received May 1, 2024 / Accepted June 10, 2021
Corresponding author: Dejan Mirković
University of Niš, Faculty of Electronic Engineering, Department of Electronics, Aleksandra Medvedeva 14, 18000 Niš, Republic of Serbia
E-mail: dejan.mirkovic@elfak.ni.ac.rs

challenging due to a nearly infinite range in signal values and verity of functions that the circuit may implement.

In general, two systematic approaches are usually employed in testing and design of analog circuits. The first is known as the simulation-before-test (SBT) where the circuit under test (CUT) with the defect is simulated and the response of the circuit is recorded [3]. After the set of faulty circuits is simulated, the fault dictionary containing responses of the fault-free (FF CUT) and faulty circuits is formed. Based on the comparison between these responses the presence of the defect can be detected. SBT allows designers to identify and rectify potential issues in the design phase before physical prototypes are built, saving time and resources. The second approach is simulation-after-test (SAT) which provides insights into how the system performs under actual operating conditions, helping to identify discrepancies between simulation and reality. However, SAT is typically performed after the design has been finalized, limiting the opportunity for early detection and correction of design flaws. SAT approach involves expenses related to equipment, materials, and personnel, which can significantly increase development costs [4]. Therefore, SBT is usually favored over the SAT in early phases of testing since it is more flexible and less expensive to apply. In this work the SBT approach is adopted, as well.

The defects in the circuits are classified as the hard (catastrophic) and the soft (parametric) defects [5]. All defects that are radically changing the topology of the circuit are considered as hard defects. These defects are the result of the physical destruction of the component and/or connection between components (over-loading, systematic design errors, extreme working conditions etc.). Accordingly, hard defects are modeled as short circuits between nodes and open circuits of connection paths. When a hard defect is present in the circuit, significant degradation of the CUT performance is expected leading to permanent malfunction. On the other hand, soft defects do not jeopardize the CUT's functionality. Usually, only some properties are outside the specified limits (e.g. speed, bandwidth, power consumption, etc.), but the circuit still preserves its function. Soft defects can arise due to the component aging or suboptimal operational conditions such as variations in ambient temperature. For the circuit analysis the soft defects are modeled as the change in component value which lies outside the tolerance range.

When testing the analog circuitry several topics should be addressed. One would be in which domain to analyze the response of the circuit (DC, frequency, time, etc.). There is also a selection of the test point i.e. where the acquisition of the desired signal will take place. The availability of the test point sometimes cannot be easily ensured. One of the most challenging is the synthesis of the input test signal. Unlike with the digital circuitry, where only one format of the test vector is available (array of bits), with analog, there is a myriad of waveform shapes that can be applied as the test signal. Therefore, it is always interesting and challenging to consider the methodologies that guarantee the testing quality while requiring the fewest modification of the system. One such methodology is the Oscillation-Based Testing (OBT) [6],[7]. Several authors confirmed the value and usability of this technique in analog and mixed-signal filtering circuitry. In [8] the OBT technique was successfully applied to wideband current conveyer filters, and can be implemented as the Built-in Self-Test structure in Very-Large Scale Integrated circuits (VLSI) [9], [10]. The efficiency of OBT is in the fact that there is no need for the input test signal i.e. problem of the test signal synthesis is circumvented. Also, only one test point, usually the output of the CUT, is enough to observe the effect of the defects in the CUT. After the OBT is applied the diagnosis of the defects can be performed as shown in [11].

The key idea behind OBT is to turn CUT into an oscillator [12]. To achieve this, one must provide some form of positive feedback in the system. This can be done in a verity of ways depending on the CUT transfer function. For the discrete time systems, like in [13], it is usually not possible to find closed form solution for the loop gain, but if the system is linear, there is a possibility to find the appropriate feedback transfer function which will enable sustained oscillations in the system. Therefore, the prime goal of this paper is to examine these possibilities for the three, second-order, filter transfer functions, namely: low-pass (LP), high-pass (HP) and band-pass (BP). Unlike the [14], where the comprehensive set of self-tuning active filters is covered, or the [15] where novel LC ladder passive network is presented, in this paper only the Sallen-Key RC realizations are considered [16],[17]. All filter, and feedback, circuits are designed with the realistic model of the operational amplifier targeting 180nm CMOS process node.

The rest of the paper is organized in six sections. The second section will cover the basic theoretical background of the OBT methodology with the emphasis on filters application. Here, the appropriate feedbacks for the three examined filter structures will be discussed from the theoretical point of view. In the third section, the circuit realization of the OBT structures for the examined filters will be presented. The structures for the OBT of the band-pass (BP) filter will undergo additional testing using intentionally introduced defects. This process aims to illustrate the practical application of the OBT methodology alongside the newly proposed feedback transfer functions. The defects modeling for circuit simulation will be discussed in the fourth section. The fifth section will cover the simulation results and discussion regarding the theoretical and practical considerations. Finally, in the conclusion, key findings will be outlined.

2. THE OBT FEEDBACK TRANSFER FUNCTIONS

To get the insight into the working principle of the OBT, the basic theoretical background will be briefly covered. Fig. 1 shows the general system with single positive feedback.

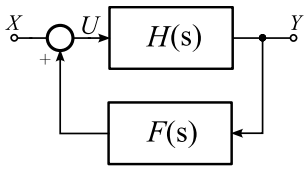

Fig. 1 General structure of the system with single positive feedback

Transfer function of the filter is denoted with $H(s)$ while the transfer function of the feedback is denoted with $F(s)$. The overall transfer function of the system is given by,

$$T(s) = \frac{Y}{X} = \frac{H(s)}{1 - F(s)H(s)} \tag{1}$$

By observing (1), it can be concluded that the system becomes instable when loop gain $F(s)H(s)$ approaches unity. According to the Barkhausen stability criterion there are two simultaneous conditions that push the system toward the instability,

$$\left|F(j\omega)H(j\omega)\right| = 1 \tag{2}$$

$$\angle\left\{F(j\omega)H(j\omega)\right\} = 2k\pi, k = 0,1,2,\ldots \tag{3}$$

i.e. the magnitude of the loop gain equals one and the phase is the integer multiple of the 2π radians [18]. The conditions (2) and (3) are usually used when analyzing the oscillators in the electronic circuits. On the other hand, one can also use the null of the system's determinant when $F(s)$ and $H(s)$ cannot be easily determined in the circuit. The system given in Fig. 1 can be described in a matrix form as,

$$\begin{bmatrix} 1 & -H(s) \\ -F(s) & 1 \end{bmatrix}\begin{bmatrix} Y \\ U \end{bmatrix} = \begin{bmatrix} 0 \\ X \end{bmatrix} \tag{4}$$

where the determinant of the system is $\Delta(s)=1 - F(s)H(s)$. For $F(s)H(s) = 1$,

$$Re\left\{\Delta(j\omega)\right\} = 0 \tag{5}$$

$$Im\left\{\Delta(j\omega)\right\} = 0 \tag{6}$$

i.e. real and imaginary part of the system's determinant simultaneously equals to zero. Therefore, either conditions (2) and (3) or (5) and (6) can be used as the theoretically well-established methods to relate the stability conditions and circuit's parameters. It should be noted that, when oscillator circuits are considered, like in OBT, there is no input signal i.e. $X=0$. It means that the system given in (4) may have infinite number of solutions or no solution [19]. However, by careful selection of the circuit parameters, one of the solutions can be ensured, i.e. sustained oscillations should be possible.

The choice of $F(s)$ strongly depends on the $H(s)$. The second-order low-pass and high-pass filter general transfer function is,

$$H_{LP}(s) = G\frac{1}{\left(s^2/\omega_0^2 + s/(Q\omega_0) + 1\right)}, \tag{7}$$

where G is the low-frequency gain of the filter, Q is the quality factor, and ω_0 is the cutoff angular frequency of the filter. The phase characteristic of the low-pass transfer function (7) is given with,

$$\angle\left\{H_{LP}(j\omega)\right\} = -\operatorname{atan}\left(\frac{\omega/(Q\omega_0)}{1-\omega^2/\omega_0^2}\right). \tag{8}$$

As the frequency ω approaches ω_0, (8) converges to the $-\pi/2$. To obtain the frequency of oscillations in vicinity of ω_0 feedback transfer function should introduce additional $\pi/2$ phase shift to fulfill the condition (3) for $k=0$. This can be achieved with the first order all-pass transfer function of a form,

$$F_{LP}(s) = -\frac{1 - s/\omega_0}{1 + s/\omega_0}, \tag{9}$$

which gives the following phase response,

$$\angle\{F_{LP}(j\omega)\} = \pi - 2\,\mathrm{atan}(\omega/\omega_0). \tag{10}$$

Similarly, for the second order high-pass transfer function,

$$H_{HP}(s) = G\frac{s^2/\omega_0^2}{\left(s^2/\omega_0^2 + s/(Q\omega_0) + 1\right)}, \tag{11}$$

with phase response,

$$\angle\{H_{HP}(j\omega)\} = \pi - \mathrm{atan}\left(\frac{\omega/(Q\omega_0)}{1 - \omega^2/\omega_0^2}\right), \tag{12}$$

the appropriate $F(s)$ would be the sign inverted (9), i.e.,

$$F_{HP}(s) = \frac{1 - s/\omega_0}{1 + s/\omega_0}, \tag{13}$$

$$\angle\{F_{HP}(j\omega)\} = -2\,\mathrm{atan}(\omega/\omega_0). \tag{14}$$

In case of a high-pass filter, the feedback provides additional $-\pi/2$ of the phase shift, to compensate for the $\pi/2$ obtained in (12) when ω approaches ω_0. In (11), G represents the high-frequency gain of the filter.

The general form of the second order band-pass filter transfer function and associated phase response are,

$$H_{BP}(s) = G\frac{s/\omega_0}{\left(s^2/\omega_0^2 + s/(Q\omega_0) + 1\right)} \tag{15}$$

$$\angle\{H_{BP}(j\omega)\} = \frac{\pi}{2} - \mathrm{atan}\left(\frac{\omega/(Q\omega_0)}{1 - \omega^2/\omega_0^2}\right). \tag{16}$$

According to (16), in a vicinity of ω_0, condition (3) is automatically fulfilled. Therefore, the simple unity feedback should be enough to open the possibility for sustained oscillations, i.e. $F_{BP}(s) = 1$. In this case ω_0 is the central frequency of the filter, and the expected gain for $\omega = \omega_0$ is $G_0 = GQ$.

The influence of the proposed $F(s)$ to the $H(s)$ is illustrated in Fig. 2 where the frequency responses of the open loop transfer functions, $H(s)F(s)$, are shown. All examples are given for the $f_0=\omega_0/(2\pi)$ =10kHz.

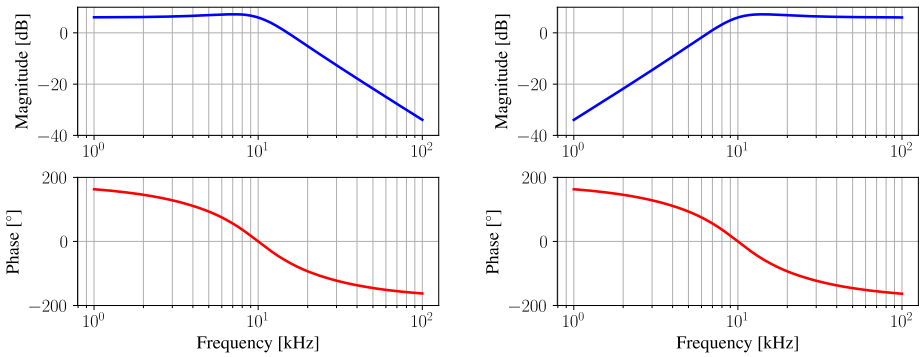

a) $H_{LP}(s)F_{LP}(s)$, G=2, Q=1 b) $H_{HP}(s)F_{HP}(s)$, G=2, Q=1

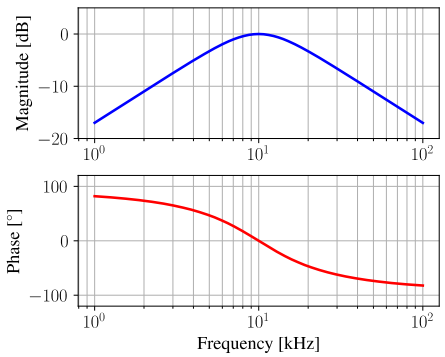

c) $H_{BP}(s)F_{BP}(s)$, G=2/√2, Q=√2/2, G_0=1

Fig. 2 Frequency responses of the $F(s)H(s)$ for a) LP, b) HP and c) BP cases, $f_0 = \omega_0/(2\pi)$ =10kHz

As can be seen from Fig. 1a and Fig. 1b the introduced all-pass $F(s)$ ensures the zero crossing of phase for the LP and HP filters at the $\omega = \omega_0$. This is also the case for the BP filter with unity feedback shown in Fig. 1c. For all three cases LP, HP, and BP there is a continuous, monotonic, phase response. By now only the phase response is considered i.e. the proposed feedback transfer functions are derived with respect to the phase responses only (condition (3)). To achieve the sustained oscillations, condition (2) must also be met, i.e. there must be enough gain/attenuation in the loop. This is the part that will be determined experimentally by adjusting the gain of the filter. The gain will be held in the allowed boundaries to keep the filter in the stable state when proposed $F(s)$ is not applied. As it will be discussed in the next section, for the examined circuit realizations, G and Q parameters are mutually dependent thus by choosing one, the other is automatically determined.

3. CIRCUIT REALIZATION OF THE OBT STRUCTURES

In this section circuit realization of the proposed OBT structures will be discussed. The LP, HP and BP have the Sallen-Key topologies. To obtain highly realistic simulation results, the model of the operational amplifier (opamp) designed for the 180nm CMOS technology process is utilized. The internal topology of the employed opamp is shown in Fig. 3. The topology contains the folded cascode input stage (transistors M1-M12) and inverter-based class-AB output stage (transistors M13 and M14) biased with the floating voltage reference source (transistors M15-M18). The BP1-3 and BN1-3 are the voltage biasing points for the entire opamp [20]. The opamp is internally compensated with the C_1=C_2=1.2pF and R=1.5kΩ. The nominal power supply voltage for the 180nm technology is 1.8V and the common-mode voltage for the signals is set to V_{CM}=1V.

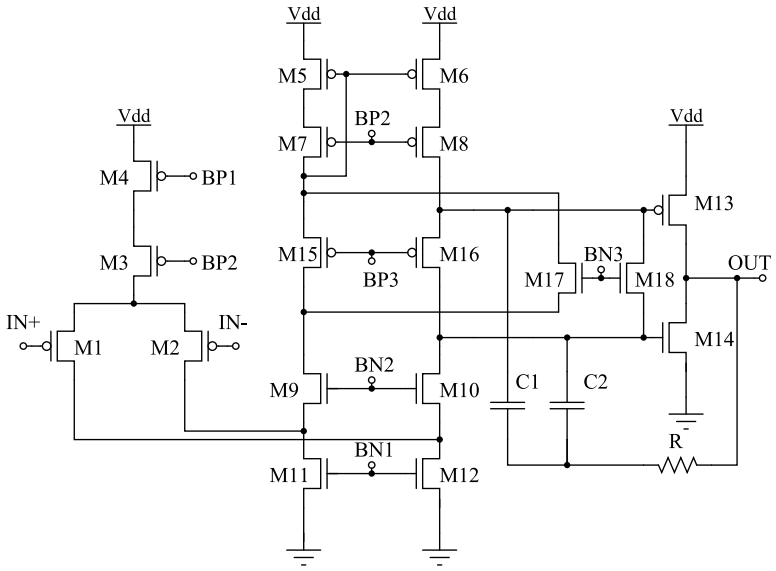

Fig. 3 The schematic of the opamp model used in realization of the OBT filter structures

Table 1 summarizes the key opamp parameters, where the DC-gain (A_{DC}), gain-bandwidth product (*GBW*), phase margin (*PM*), settling time (t_s) and slow-rate (*SLR*), are given for the unity-gain configuration. The opamp itself will introduce some phase shift as well. However, this should not contribute significantly to the overall loop phase shift since The Gain-Bandwidth Product (GBW) exceeds the target Oscillation-Based Testing (OBT) oscillation frequency, f_0, by three orders of magnitude, where f_0 is set at 10kHz. Therefore, in further derivations of the circuit transfer functions opamp will be considered as an ideal.

Table 1 The key opamp parameters

A_{DC} [dB]	*GBW* [MHz]	*PM* [°]	t_s [ns]	*SLR* [V/μs]
103.16	38.72	58.80	268.46	23.72

The proposed circuit realization of the OBT structures for the LP and HP filters are shown in Fig. 4a and Fig. 4b, respectively. The test mode is selected by setting the switch at the position 1. The normal mode of operation is for the switch position 0.

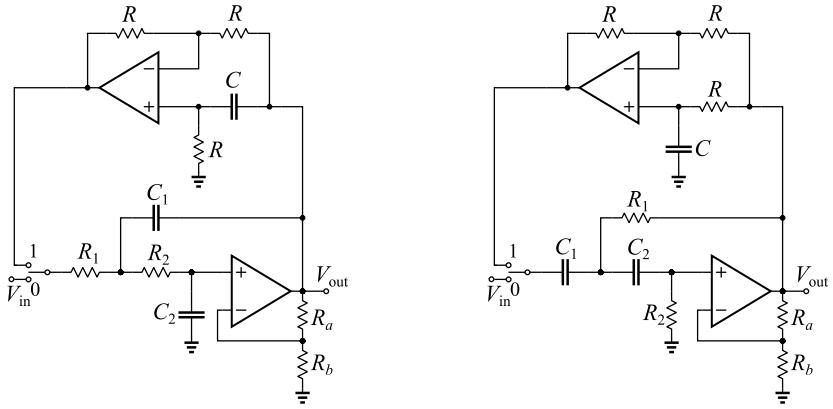

a) LP OBT b) HP OBT

Fig. 4 The OBT structures for the LP and HP filters

As suggested in (9) and (13) the first order all-pass filters are connected between the output node (V_{out}) and the switch node 1. Assuming an ideal opamp the transfer functions of first-order all-pass filters are,

$$F_{LP,HP}(s) = p \cdot \frac{1 - sRC}{1 + sRC}, p = \begin{cases} -1 & for\ LP \\ 1 & for\ HP \end{cases} \tag{19}$$

According to (19) the RC constant should satisfy the relation, $\omega_0=1/(RC)$. The general form of Q and ω_0 for the LP and HP filters from Fig. 4 are,

$$\omega_0 = \frac{1}{\sqrt{C_1 R_1 C_2 R_2}}, Q = \begin{cases} \left[(1-G)\sqrt{\frac{R_1}{R_2}\frac{C_1}{C_2}} + \left(\sqrt{\frac{R_1}{R_2}} + \sqrt{\frac{R_2}{R_1}} \right) \sqrt{\frac{C_2}{C_1}} \right]^{-1} & for\ LP \\ \left[(1-G)\sqrt{\frac{R_2}{R_1}\frac{C_2}{C_1}} + \left(\sqrt{\frac{C_2}{C_1}} + \sqrt{\frac{C_1}{C_2}} \right) \sqrt{\frac{R_1}{R_2}} \right]^{-1} & for\ HP \end{cases}, \tag{20}$$

where, $G = 1 + R_a/R_b$. Since the prime goal is the proof-of-concept i.e. to force the CUT to oscillate, following simplifications are made, $R_1=R_2=R$, $C_1=C_2=C=1/(\omega_0 R)$ leaving the R_a/R_b as the free parameter that sets both, G and Q of the filter. For this choice of component values, G should be smaller than three to keep the filter stable since, $Q=1/(3 - G)$.

The proposed OBT structure for the BP filter is shown in Fig. 5. According to (16) only unity feedback should be applied.

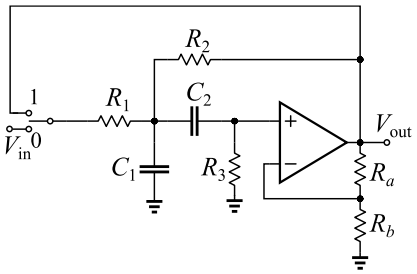

Fig. 5 The OBT structures for the BP filter

The Q and ω_0 for the BP shown in Fig. 5 are,

$$\omega_0 = \frac{1}{\sqrt{C_1(R_1 \parallel R_2)C_2R_3}}, Q = \omega_0\left[\frac{1}{C_2R_3} + \frac{1}{C_1R_1}\left(1+\frac{R_1}{R_3}+(1-G)\frac{R_1}{R_2}\right)\right]^{-1}, \quad (21)$$

Selecting the R_1=R_2=R and C_1=C_2=C, results with the ω_0=√2/(RC) and Q =√2/(4 – G). The filter's stability is preserved for the G smaller than four.

4. Defects Modeling For Circuit Simulation

To demonstrate the application of the proposed OBT structures one of them will be additionally analyzed by introducing defects into the passive components. The BP OBT structure is chosen for this purpose. Two types of hard defects are introduced namely, the stack-at-short (SAS) and the stack-at-open (SAO). In the circuit simulation, the SAS is modeled by setting the small resistance of 1mΩ across the component terminals while the SAO is modeled by the large resistance of 1TΩ in series with the component. The extremely small resistance value of 1mΩ ensures that the voltage drop for the expected mA currents will be in the sub μV range that can be considered as a short circuit. Also, 1TΩ resistances should keep the currents in pA range for voltages of the order of 1V modeling the open circuit.

Considering that the variation of the on-chip resistances and capacitances is very large (about 20%), the significant amount of component value change must be introduced to provoke the soft defect [21]. Since on-chop components are realized as the polygons of the certain width, W, and lengths, L, the soft defects are modeled by relating the ±50% change of component dimensions (W and/or L) to the component value. It is important to note that the resistance value is proportional to the L/W ratio and that the capacitance value is proportional to the WL product. E.g. changing the L and W in the same direction by the same amount will not influence the resistance but will influence the capacitance value. On the other hand, by changing the L and W in the opposite directions by the same amount will not influence the capacitance value (area stays the same) but it will influence the resistance value. Therefore, adopted absolute change in the resistance and capacitance values from the nominal one are ΔR = [−67%, −50%, −33%, 50%, 100%, 200%] and ΔC = [−75%, −50%, 50%, 125%], respectively. In total there are six soft defects for each resistor and four for each capacitor. Since, BP filter contains five resistors and two capacitors the total number of the soft defects is thirty-eight. Considering two hard defects per component the total number of hard defects is fourteen.

5. SIMULATION RESULTS

The SPICE simulation results for the OBT structures of the LP, HP and BP filters are shown in Fig. 6. The waveforms of the output voltage, V_{out}, are given in subfigures a), c) and e) while the corresponding spectrum, obtained from 4096-point FFT, is given in subfigures b), d) and f). Based on the waveforms, it takes about 0.4ms for the OBT structures to start oscillating. It can be concluded that the theoretical assumptions regarding the proposed feedback transfer functions are valid.

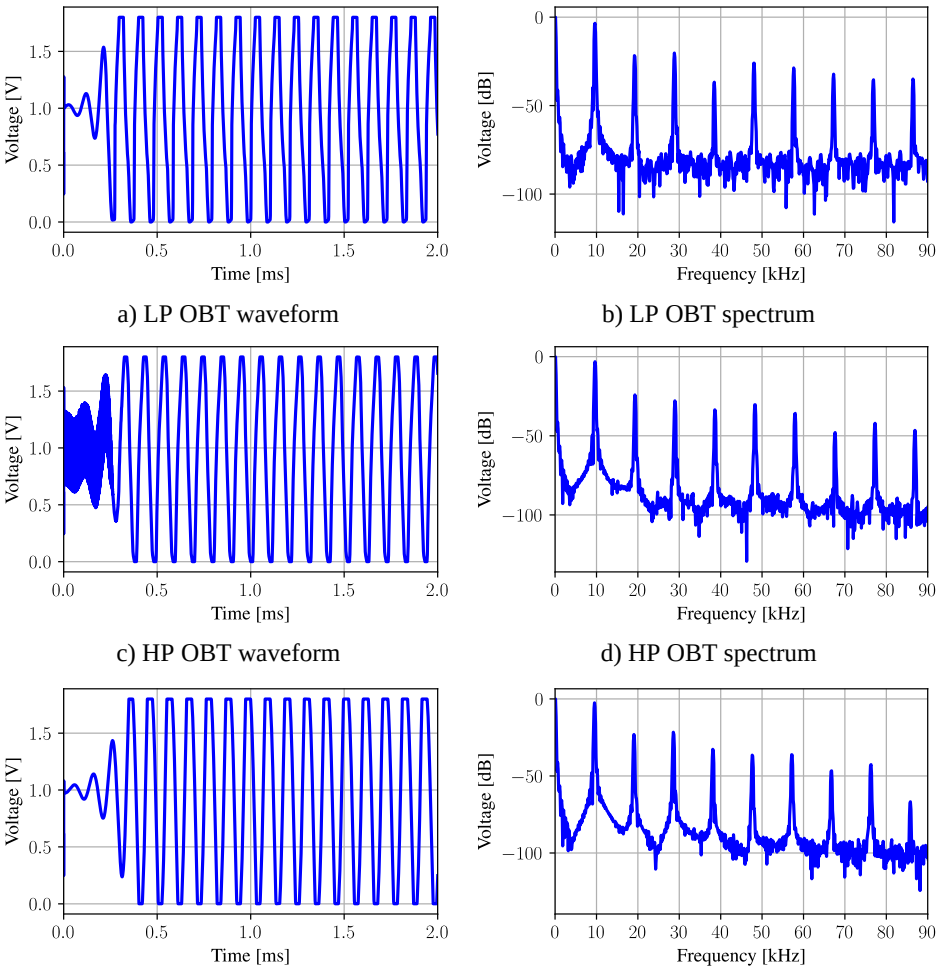

a) LP OBT waveform

b) LP OBT spectrum

c) HP OBT waveform

d) HP OBT spectrum

e) BP OBT waveform

f) BP OBT spectrum

Fig. 6 The simulation results for the LP, HP, and BP OBT structures

The columns two through four in Table 2 summarize the most-commonly observed parameters for the FF CUT when OBT is applied. These parameters are, oscillating frequency, f_0, output voltage amplitude, V_{out}, the total-harmonic distortion, *THD* (calculated up to 10th

harmonic) and average supply current, I_{DD}. Due to the component non-idealities, obtained oscillating frequency slightly differs from the target 10kHz.

Table 2 The OBT parameters for the FF CUT in test mode

CUT	f_0 [Hz]	V_{out} [mV]	THD* [%]	I_{DD} [mA]	G	Q	C [pF]	R [kΩ]	R_a [kΩ]
LP	9645	900	22.37	1.296	2	1	45	350	50
HP	9645	900	12.70	1.407	2	1	45	350	50
BP	9564	900	12.43	1.192	2.25	0.808	60	375	62.5

* Calculated up to 10th harmonic

The values of the G and Q are given in the sixth and seventh column, respectively. The nominal values of the components are given in the last three columns. R_b is set to 50kΩ in each realization. Since the integrated circuits implementation is intended, relatively large value is chosen for R to keep the values of C in pF range ($\omega_0 \propto 1/(RC)$).

The complete fault dictionary for fourteen hard defects introduced into the BP OBT structure is given in Table 3. The first two columns contain the component name and the defect type. The rest of the columns contains the observed parameters. The defects are detected by tracking the deviation between parameters of the FF CUT and the faulty CUT.

Table 3 The fault dictionary for hard defects of the BP OBT structure

Comp.	Defect	f_0 [Hz]	V_{out} [V]	I_{DD} [A]	THD [%]
C_1	SAO	187.08E+3	899.77E-3	430.72E-6	7.08
C_2	SAO	-	10.88E-15	1.192E-3	-
R_1	SAO	-	6.83E-15	1.192E-3	-
R_2	SAO	-	115.77E-18	147.64E-6	-
R_3	SAO	-	249.80E-15	1.192E-3	-
R_a	SAO	-	62.01E-15	1.192E-3	-
R_b	SAO	1.32E+3	900.00E-3	188.11E-6	25.55
C_1	SAS	-	5.27E-15	1.192E-3	-
C_2	SAS	-	1.89E-15	199.27E-6	-
R_1	SAS	14.96E+3	899.77E-3	516.28E-6	44.68
R_2	SAS	-	3.77E-15	1.192E-3	-
R_3	SAS	18.14E+3	899.77E-3	188.78E-6	9.38
R_a	SAS	1.33E+3	899.65E-3	194.89E-6	25.39
R_b	SAS	-	62.51E-15	1.192E-3	-

The hard defects classification for the BP OBT structure is presented in Table 4. The total coverage is 100% since the effect of all introduced defects is such that changes one or more of the observed parameters of the FF CUT. Two classes of the response are identified: Oscillations and No-oscillations. The Oscillations class covers the defects that do not change the oscillation frequency of the OBT structure but changes one of the other observed parameters (V_{out}, THD or I_{DD}). The No-oscillation class contains the defects that do not allow oscillations (denoted with a dash in the frequency and THD columns of Table 3). In the case of the BP OBT structure there are five defects in Oscillation class and they can be detected by THD or the I_{DD} deviation from the same parameters of the FF CUT given in Table 2 (BP row).

There are nine defects in the No-oscillation class, where two of them can be detected by the deviation of I_{DD} (R_2 SAO and C_2 SAS) and five cannot be diagnosed since they produce no change in the power supply current, I_{DD}.

Table 4 Classification of hard defects for the BP OBT structure

Response class	Oscillations	No oscillations	
Diagnosed	by frequency, THD or current	by current	Undiagnosed
Number	5	2	7
Percentage	35.71%	14.29%	50.00%

The fault dictionary for the soft defects in resistors and capacitors of the BP is presented in Tables 5 and 6, respectively. Again, 100% coverage is achieved. In this case the fifty-fifty split between Oscillations and No-oscillations classes is identified as summarized in Table 7.

Table 5 The fault dictionary for soft defects in resistors of the BP OBT structure

Comp.	ΔR [%]	f_0 [Hz]	V_{out} [V]	I_{DD} [A]	THD [%]
R_1	200	-	156.60E-15	1.192E-3	-
	100	-	74.95E-12	1.192E-3	-
	50	-	18.80E-6	1.192E-3	-
	-33	9.75E+3	899.70E-3	954.000E-6	4.14
	-50	10.35E+3	899.80E-3	818.700E-6	15.67
	-67	11.00E+3	899.80E-3	714.700E-6	32.51
R_2	200	4.11E+3	899.80E-3	474.500E-6	20.27
	100	5.62E+3	899.80E-3	598.600E-6	16.83
	50	6.96E+3	899.80E-3	754.500E-6	22.93
	-33	-	319.90E-15	1.192E-3	-
	-50	-	142.30E-15	1.192E-3	-
	-67	-	67.34E-15	1.192E-3	-
R_3	200	-	443.30E-15	1.192E-3	-
	100	-	35.92E-12	1.192E-3	-
	50	-	7.98E-6	1.192E-3	-
	-33	10.00E+3	899.80E-3	805.300E-6	20.21
	-50	10.64E+3	899.80E-3	651.200E-6	8.89
	-67	11.50E+3	899.80E-3	511.000E-6	29.17
R_a	200	-	148.40E-15	1.192E-3	-
	100	-	254.70E-15	1.192E-3	-
	50	-	592.60E-15	1.192E-3	-
	-33	8.42E+3	899.70E-3	673.200E-6	19.14
	-50	7.61E+3	899.70E-3	516.700E-6	15.00
	-67	6.43E+3	899.70E-3	365.800E-6	26.31
R_b	200	96.42E+3	899.90E-3	352.000E-6	22.38
	100	7.58E+3	899.80E-3	510.000E-6	20.73
	50	8.49E+3	899.80E-3	676.400E-6	25.32
	-33	-	597.40E-15	1.192E-3	-
	-50	-	274.10E-15	1.192E-3	-
	-67	-	156.20E-15	1.192E-3	-

One half of soft defects does not produce oscillations but preserve the same I_{DD} as the FF CUT (undiagnosed). The other half of soft defects keeps the OBT structure in the oscillation state and can be diagnosed by deviation in frequency, THD or I_{DD}. Finally, for a better insight the classification results given in Tables 4 and 7 are presented graphically in Fig. 7

Table 6 The fault dictionary for soft defects in capacitors of the BP OBT structure

Comp.	ΔC [%]	f_0 [Hz]	V_{out} [V]	I_{DD} [A]	THD [%]
C_1	125	-	155.00E-15	1.192E-3	-
	50	-	227.50E-9	1.192E-3	-
	-50	11.70E+3	899.80E-3	778.900E-6	6.88
	-75	13.89E+3	899.80E-3	624.800E-6	17.04
C_2	125	5.61E+3	899.80E-3	760.500E-6	17.35
	50	7.27E+3	899.80E-3	910.700E-6	3.42
	-50	-	189.10E-15	1.192E-3	-
	-75	-	60.73E-15	1.192E-3	-

Table 7 Classification of soft defects for the BP OBT structure

Response class	Oscillations	No oscillations
Diagnosed	by frequency, THD or current	Undiagnosed
Number	19	19
Percentage	50.00%	50.00%

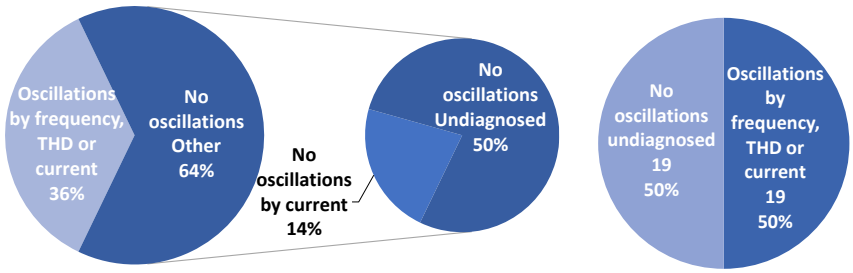

a) Hard defects b) Soft defects

Fig. 7 The share of the diagnosed/undiagnosed defects in the response classes for the BP OBT structure

6. CONCLUSION

In this paper, possible solutions for the feedback transfer functions applied in OBT test structures of active RC filters are examined. The proposed feedback transfer functions are successfully applied to three types of second-order Sallen-Key filters LP, HP, and BP. The solutions are derived according to the phase responses of the examined filters.

For each examined filter the key relations between filters' cut-off/central frequency, *Q* factor and the gain *G*, are derived. Based on these relations an appropriate strategy for selecting the values of the circuit's elements is given.

The proposed OBT structures are custom designed targeting the 180nm CMOS process. The internal topology and main characteristics of the opamp are presented. The opamp is designed with the goal of minimizing its influence on the overall frequency characteristics of the filter. The theoretical assumptions regarding proposed feedback functions are confirmed with the SPICE simulations showing that all three of the proposed OBT structures oscillate at the filters cut-off/central frequency.

The OBT is further demonstrated on the OBT BP structure where total of fourteen hard and thirty-eight soft defects are introduced into the BP passive components. In both cases 100% defect coverage is achieved. For better insight the defects are classified first by the response type, and then by the parameter that can be used for the defect diagnosis.

There are two main contributions of this work. Firstly, it is the introduction of the all-pole transfer functions in the LP and HP OBT structures which enabled the oscillation frequency near the filters' cut-off frequency. These cases are not previously examined in [11] and [13]. Secondly, based on the simulation results for the BP OBT structure, it was shown that tracking the power-supply current as an additional parameter to the output voltage waveform and spectrum, improvements in the defects diagnosis can be achieved (e.g. 14% in the No-oscillations class, for hard defects, Fig. 7a). In the future work the proposed methodology could be applied to different circuit topologies with the goal of exploring the possibilities for the defects' detection and diagnosis.

Acknowledgement: *This work has been supported by the Ministry of Education, Science and Technological Development of the Republic of Serbia.*

REFERENCES

[1] G. Q. Zhang, M. Graef, and F. van Roosmalen," The rationale and paradigm of "more than Moore", *56th Electronic Components and Technology Conference 2006*, San Diego, CA, USA, 2006, pp. 7, doi: 10.1109/ECTC.2006.1645639.

[2] S. Qamar, W. H. Butt, M. W. Anwar, F. Azam, and M. Q. Khan, "A Comprehensive Investigation of Universal Verification Methodology (UVM) Standard for Design Verification," *Proceedings of the 2020 9th International Conference on Software and Computer Applications*, 2020, pp. 339–343, doi: 10.1145/3384544.3384547.

[3] M. Karmani, C. Khedhiri, B. Hamdi, and B. Bensalem, "A Fault Dictionary-Based Fault Diagnosis Approach for CMOS Analog Integrated Circuits," *International Journal of VLSI Design & Communication Systems*, vol. 2, no. 3, 2011, doi: 10.5121/vlsic.2011.2301.

[4] D. Monda, G. Ciarpi, and S. Saponara, "Diagnosis of faults induced by radiation and circuit-level design mitigation techniques: Experience from vco and high-speed driver cmos ics case studies," *Electronics (Switzerland)*, vol. 10, no. 17, 2021, doi: 10.3390/electronics10172144.

[5] D. Perry, M. Nakamoto, N. Verghese, P. Hurat, and R. Rouse, "Model-based approach for design verification and co-optimization of catastrophic and parametric-related defects due to systematic manufacturing variations," *Design for Manufacturability through Design-Process Integration*, 2007. doi: 10.1117/12.712471.

[6] K. Arabi and B. Kaminska, "Oscillation-test methodology for low-cost testing of active analog filters," *IEEE Trans Instrum Meas*, vol. 48, no. 4, pp. 798–806, 1999, doi: 10.1109/19.779176.

[7] M. Milić, M. A. Stošović, and V. Litovski, "Oscillation based analog testing A case study," Proceedings of the 34th International Convention on Information and Communication Technology, Electronics and Microelectronics – MIPRO, vol. 1, pp. 118-123, May, 2011, ISBN 1847-3938.

[8] P. Petrashin, L. Toledo, W. Lancioni, P. Osuch, and T. Stander, "Oscillation-Based Test Applied to a Wideband CCII," *VLSI Design*, vol. 2017, 2017, doi: 10.1155/2017/5075103.
[9] M. Ballot and T. Stander, "A RF amplifier with oscillation-based BIST based on differential power detection," *Proceedings - IEEE International Symposium on Circuits and Systems*, 2021. doi: 10.1109/ISCAS51556.2021.9401388
[10] H. P. Nel, T. Stander, and F. C. Dualibe, "Built-In Oscillation-Based Self-Testing of a 2.4 GHz LNA in 0.35µ m CMOS," *2018 25th IEEE International Conference on Electronics Circuits and Systems, ICECS 2018*, 2018. doi: 10.1109/ICECS.2018.8618052.
[11] M. A. Stošović, M. Milić, and V. Litovski, "Analog filter diagnosis using the oscillation based method," *Journal of Electrical Engineering*, vol. 63, no. 6, 2012, doi: 10.2478/v10187-012-0052-4.
[12] M. Petrovic and M. Milic, "Analog Device Design for Testability in the Case of Oscillation Based Testing," *Proceedings of the International Conference on Microelectronics, ICM*, 2017. doi: 10.1109/MIEL.2017.8190122.
[13] M. Milic and V. Litovski, "Oscillation-based testing method for detecting switch faults in High-Q SC biquad filters," *Facta Universitatis, Series: Electronics and Energetics*, vol. 28, no. 2, 2015, doi: 10.2298/fuee1502223m.
[14] D. Mitić, G. Jovanović, M. Stojčev, and D. Antić, "On Design of Self-tuning Active Filters," *Facta Universitatis, Series: Automatic Control and Robotics*, vol. 19, no. 1, 2020, doi: 10.22190/fuacr2001059m.
[15] D. Živaljević and S. V. Nikolić, "New Type of Nearly Monotonic Passband Filters with Sharp Cutoff," *Facta Universitatis, Series: Automatic Control and Robotics*, vol. 16, no. 1, 2017, doi: 10.22190/fuacr1701061z.
[16] R. P. Sallen and E. L. Key, "A practical method of designing RC active filters," *IRE Transactions on Circuit Theory*, vol. 2, no. 1, 1995, doi: 10.1109/tct.1955.6500159.
[17] V. Litovski, "Active RC Cascade Circuit Synthesis," in Lecture Notes in Electrical Engineering, vol. 596, 2019. doi: 10.1007/978-981-32-9852-1_15.
[18] L. Von Wangenheim, "On the Barkhausen and Nyquist stability criteria," *Analog Integrated Circuits and Signal Processing*, vol. 66, no. 1, 2011, doi: 10.1007/s10470-010-9506-4.
[19] A. G. S. Ventre, "Determinants and Systems of Linear Equations," in *Calculus and Linear Algebra*, (2023). doi: 10.1007/978-3-031-20549-1.
[20] M. P. Garde, A. Lopez-Martin, R. G. Carvajal, and J. Ramírez-Angulo, "Super Class-AB Recycling Folded Cascode OTA," *IEEE J Solid-State Circuits*, vol. 53, no. 9, 2018, doi: 10.1109/JSSC.2018.2844371.
[21] D. D. Mirkovic, M. J. Stanojlovic Mirkovic, M. L. J. Milic, and V. Z. Petrovic, "A Defects Classification Algorithm for the Hybrid OBT–IDDQ Fault Diagnosis Technique in Analog CMOS Integrated Circuits," *Journal of Circuits, Systems and Computers*, vol. 0, no. 0, p. 2450146, doi: 10.1142/S0218126624501469.